

One-pot electrodeposition, characterization and photoactivity of stoichiometric copper indium gallium diselenide (CIGS) thin films for solar cells†‡§

Mohammad Harati,^{ab} Jia Jia,^a Kévin Giffard,^a Kyle Pellarin,^a Carly Hewson,^a David A. Love,^{bc} Woon Ming Lau^{ab} and Zhifeng Ding^{*ab}

Received 16th May 2010, Accepted 9th August 2010

DOI: 10.1039/c0cp00586j

Herein we report the one-pot electrodeposition of copper indium gallium diselenide, $\text{CuIn}_{1-x}\text{Ga}_x\text{Se}_2$ (CIGS), thin films as the p-type semiconductor in an ionic liquid medium consisting of choline chloride/urea eutectic mixture known as Reline. The thin films were characterized by scanning electron microscopy with energy dispersive X-ray analysis, transmission electron microscopy, X-ray photoelectron spectroscopy, Raman microspectroscopy, and UV-visible spectroscopy. Based on the results of the characterizations, the electrochemical bath recipe was optimized to obtain stoichiometric CIGS films with x between 0.2 and 0.4. The chemical activity and photoreactivity of the optimized CIGS films were found to be uniform using scanning electrochemical microscopy and scanning photoelectrochemical microscopy. Low-cost stoichiometric CIGS thin films in one-pot were successfully fabricated.

Introduction

Copper indium gallium diselenide, $\text{CuIn}_{1-x}\text{Ga}_x\text{Se}_2$ (CIGS, where x ranges between 0.2 and 0.4), is a promising absorbing layer for thin film solar cells. It has an adjustable band-gap in the range of 1.05–1.67 eV;¹ the absorption spectrum of CIGS thin films matches the solar spectrum better than most solar cell absorbing layers when the value of x is in the above range; and it has a large optical absorption coefficient (10^5 cm^{-1}) which results from the direct energy gap and permits thin films with the thicknesses of about 1 μm to absorb sufficient amounts of light.^{2,3} Solar cells based on CIGS absorber layers illustrate high photon to current conversion efficiencies of about 20% in a laboratory scale.⁴

Several methods of CIGS deposition based on vacuum techniques such as multi-step physical vapour deposition and conventional sputtering techniques have been developed.^{5–10} The bottleneck in the production of CIGS thin film solar cells as a renewable energy source is formed by a combination of their high manufacturing cost, difficulty in scaling up the manufacturing process due to the limited size of the vacuum chambers used for depositing these films, and difficulty in the

control on the formation of stoichiometric films. Due to the relatively high vapour pressure of selenium, even at moderately elevated temperatures, as-deposited CIGS films often do not contain the proper stoichiometric amount of selenium. Consequently, a low-cost and large-area method of deposition of stoichiometric CIGS films without post-deposition heat treatment in selenium atmosphere has not yet been fulfilled. To address some of these issues, solution-based approaches including spray pyrolysis/spray chemical vapour deposition,¹¹ precursor deposition,^{12,13} and nanocrystal printing¹⁴ have also been developed. On the whole, although CIGS devices have already been commercialized, the science and technology of CIGS films are still evolving.

It is well known that many electrically conductive materials can be deposited over large areas at a low cost using electrochemical processes; it is therefore logical to explore the electrodeposition of stoichiometric CIGS films. Electrodeposition of thin film CIGS in various solvents such as aqueous, alcohol and ionic liquid has been the subject of numerous studies. However, electrodeposition of stoichiometric CIGS requires soluble salts of all four elements and control of their reduction potentials. Several research groups have reported the electrodeposition of CIGS films in aqueous solution. Calixto *et al.* studied the influence of film deposition parameters such as bath composition, pH, deposition potential and material purity on a single-step electrodeposition of CIGS film. They reported obtaining good morphological films after annealing and selenization at a high temperature.¹⁵ More recently, a single-bath method for the production of CIGS films¹⁶ was optimized by adjusting the above parameters. Lew *et al.* reported the electrodeposition of CIGS films in an aqueous solution in the presence of LiCl as a supporting electrolyte.¹⁷ Sun and coworkers reported electrodeposition of Cu-poor and Cu-rich near stoichiometric CIGS by one-step electrodeposition process from acidic aqueous solutions.¹⁸ In yet another

^a Department of Chemistry, The University of Western Ontario, 1151 Richmond Street, London, ON N6A 5B7, Canada.

E-mail: zfding@uwo.ca; Fax: +1 519-6613022;

Tel: +1 519-6612111 ext. 86161

^b Surface Science Western, The University of Western Ontario, 1151 Richmond Street, London, ON N6A 5B7, Canada

^c Rosstech Inc., 71 15th Line South, Orillia, ON L3V 6H1, Canada

† Dedicated to Prof. Dr Gerhard Ertl for having laid the methodological foundations for modern surface chemistry.

‡ Contributed to the PCCP collection on Electrified Surface Chemistry, following the 1st Ertl Symposium on Electrochemistry and Catalysis, 11–14 April, 2010, Gwangju, South Korea.

§ Electronic supplementary information (ESI) available: Cyclic voltammetry of a Reline bath containing Cu-In-Ge-Se salts, and SEM/EDX of a CIGS film using the constant potential method. See DOI: 10.1039/c0cp00586j

approach, Zou and coworkers reported the preparation of CIGS films by a one-step electrodeposition in an alcohol solution.¹⁹ It has been found that adding a complexing agent halts the production of hydrogen and creation of pinholes, and increases composition uniformity. For instance, Feng *et al.* also reported on the co-electrodeposition of CIGS precursors in a citrate bath and followed by annealing the as-deposited films to improve the crystalline properties.²⁰ Zhao *et al.* reported a systematic cyclic voltammetry (CV) study to better understand the electrochemical behaviour during the co-deposition of Cu, In, Ga and Se in a citrate bath.^{21,22} Using another method, Tiwari *et al.* reported the fabrication of CIGS films from thiocyanate complex electrolytes.²³ Liu *et al.* reported a one-step electrodeposition process of CIGS film formation in a water–dimethylformamide (DMF) solution,² where citrate was added as the complexing agent. Basol *et al.* carried out two-step electrodeposition using tartrate and citrate as complexing agents in the alkaline regime.²⁴ According to their approach, both complexing agents are suitable to solubilize indium and gallium ions at high pH with the advantage of reduced hydrogen.

Room Temperature Ionic Liquids (RTILs) typically demonstrate a wide electrochemical window and a very low vapour pressure.^{25,26} They have found numerous applications in electrochemistry.^{27–29} A method of electrochemical deposition of CIGS in an ionic liquid was recently disclosed by Peter and

coworkers,³⁰ in which the deposition processes for the preparation of CIS and CIGS precursors were elegantly described. A constant potential of -1.35 V *versus* Pt was applied to deposit a CIGS precursor film in a Reline (an ionic liquid of choline chloride/urea eutectic mixture) bath containing 50 mM InCl_3 , 7 mM CuCl_2 , 10 mM SeCl_4 and 40–80 mM GaCl_3 . However, CIGS films thus deposited were selenium deficient, as indicated by the fact that the post-deposition treatment under selenium atmosphere was required to increase the selenium content of the films.

Scanning electrochemical microscopy (SECM)^{31,32} is a useful analysis tool in the area of chemical and biochemical kinetics,^{33–38} reactivity imaging,^{38–43} and micrometre scale structuring and reading^{44–47} at various interfaces. While photoelectrochemical systems based on semiconductor electrodes have been investigated for the conversion of solar energy to electricity, photoelectrosynthesis, photoelectrolysis and photocatalysis,^{48,49} there are a few reports on the use of SECM steady-state measurements for obtaining reactivity information about processes at an illuminated semiconductor/electrolyte interface (for instance, ref. 50). Scanning photoelectrochemical microscopy (SPECM) is a potentially powerful tool to evaluate the photoreactivity of p-type CIGS films. With the CIGS film in contact with an electrolyte solution containing a mediator, ferrocenemethanol (Fc), the SECM probe in the vicinity of the interface was biased at 0.350 V *versus* a Ag/AgCl reference electrode to ensure that Fc was oxidized to ferroceniummethanol (Fc^+) at the probe (Fig. 1). Electrons promoted to the conduction band of the CIGS film by light illumination were expected to be injected to Fc^+ , and this converted back to Fc^{48,49} (Fig. 2). The SECM probe current should thus increase in the proximity of the interface (Fig. 1), giving more positive feedback. The amount of the feedback could be a measure of the CIGS photoreactivity.

The present report provides a one-pot fabrication strategy that uses electrochemistry to generate stoichiometric CIGS films on a molybdenum electrode with no requirement of post-deposition thermal sintering. We found that Reline is at low cost (about \$6 per 100 mL) and has no unwanted reactions during electrodeposition of CIGS. For example, Reline has a potential window wide enough for the deposition of gallium and indium while this was restricted by hydronium ion reduction in water baths, which causes pinholes, lack of composition uniformity, and subsequently lowers cell efficiency.

The electrochemical bath recipe was optimized by means of various microscopic and spectroscopic investigations of the

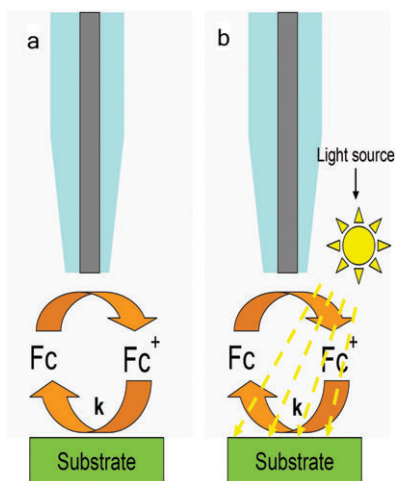


Fig. 1 Schematic diagrams of SECM setup in dark (a) and upon illumination (b).

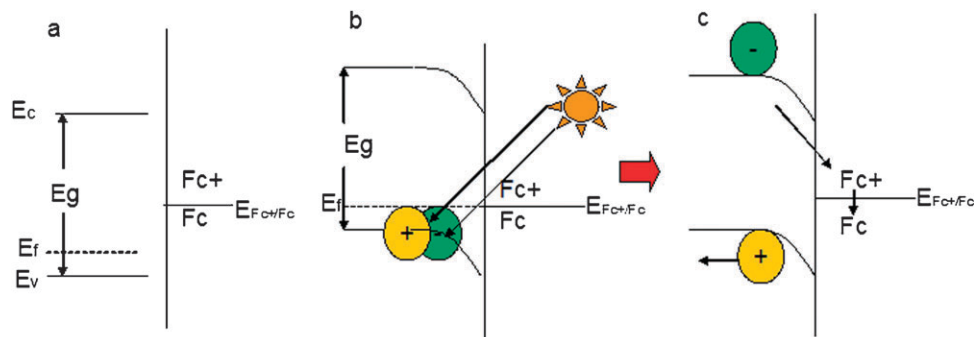


Fig. 2 The process of electron/hole formation and the reduction of Fc^+ to Fc under light.

fabricated films. This can lead to a low cost production of CIGS films that is relatively simple to scale-up from laboratory size to commercial fabrication. SECM and SPECM were used to study local properties and reactivity of the CIGS film in the dark and upon illumination.

Experimental

The glass substrate (soda lime microscopic glasses, Zefon International, Inc., Mississauga, Ontario) treatment was published elsewhere,⁴⁷ and Mo sputtering procedure followed was a routine one. Resistivity of sputtered molybdenum films were measured as $5.80 \times 10^{-8} \Omega \text{ m}$ with a four point probe (Model FPP 5000) purchased from Veeco Instrument Inc. (Plainview, NY). Electrodeposition was performed in a custom-made four-neck thermal-jacketed 50 mL glass flask using a potentiostat (Model 173) with a digital coulometer (179), and a universal programmer (Model 175) (EG&G Princeton Applied Research, Oak Ridge, TN). The voltammetry and chronoamperometry were acquired by programs written in LabVIEW (National Instruments, Austin, TX) through a computer interface (SR 245, Stanford Research, Sunnyvale, CA). The electrochemical bath contained a mixture of chloride salts of copper, indium, gallium, and selenium dissolved in Reline with the appropriate concentrations and loaded into the flask within a glove box. The counter and reference electrodes were platinum wires. The electrodeposition was conducted by scanning the applied potential between -0.2 V and -2.2 V or setting a constant potential of -1.500 V versus the Pt reference electrode. After the deposition, the substrate was removed from the electrochemical bath, rinsed with distilled water, and dried under argon flow (ultra high purity, >99%, Praxair Canada Inc., London, ON).

The film morphology was examined using a Hitachi S-4500 (Japan) field emission scanning electron microscope (FESEM) and qualitative elemental composition comparisons among different samples were made with a dispersive X-ray (EDX) analytical system. Transmission electron microscope (TEM) images were acquired with a transmission electron microscope (Philips CM 10) equipped with a field emission gun operated at 100 kV. TEM samples were prepared by embedding CIGS powder in Epon-Araldite. Embedded CIGS was ultra-cut in a trapezoid shape with a thickness of approximately 70 nm using a glass knife. The trapezoid pieces were collected from the knife area onto a Cu TEM grid. X-Ray photon spectroscopy (XPS) measurements were carried out with a Kratos Axis Ultra spectrometer (UK) with Al K α as the X-ray source. XPS data were analyzed using curve fitting which was carried out using Casa software.

UV-visible absorbance spectra were recorded with a dual-beam using a Varian Cary 100 spectrophotometer (Palo Alto, CA) in the reflection mode. The reference was Mo-coated glass. Confocal Raman microspectroscopy was measured using a WITec Raman instrument (Alpha SNOM, WITec, Germany).⁵¹

The SECM working electrodes, 10.0 μm diameter ultra-microelectrodes (UMEs) with a diameter ratio of the glass sheath to Pt (RG) of about 3, were prepared as described elsewhere.^{34,51} In brief, a 10.0 μm diameter Pt wire (Good Fellow

Cambridge Limited, Huntingdon, England) with a length of 1 cm was sealed in a glass capillary under vacuum with one end pulled and sealed. Then the Pt disk was exposed by a sanding pad (Buehler Ltd., Bluff, Illinois) attached to a rotating wheel, the electrode disk was polished in succession by polishing pads (Buehler) coated with alumina having diameters of 3.0, 0.3, and 0.05 μm , respectively. The glass sheath was sharpened by 3.0 and 0.05 μm diameter diamond pads (Buehler) until RG was about 3. An Ag/Ag₂SO₄ electrode was used as a reference electrode and a Pt wire was used as a counter electrode. The CIGS film substrate was attached to the bottom of the Teflon SECM cell.^{34,35} The film was exposed to the solution through an aperture of 5 mm in diameter. The cell held a solution containing 0.9 mM of ferrocenemethanol (Fc) (97%, Aldrich, Mississauga, Ontario), and 0.1 M Na₂SO₄ (Caledon Laboratories Ltd., Georgetown, Ontario).⁵²

A schematic of the experimental setup in dark and under light⁵⁰ is given in Fig. 1. A custom-built system was used to carry out the SECM experiments as depicted elsewhere.^{35,53,54} The position of the UME was controlled by a 3-axis positioner and controller (EXFO/Burleigh 8200 Inchworm Controller system, EXFO, Mississauga, ON). A bipotentiostat (CHI832A Electrochemical Analyzer, CH Instruments, Austin, TX) was used to control the potential applied between working electrode and reference electrode, and to measure the current. The output current and electrode coordinates were recorded and analyzed by a computer and data acquisition system.⁵² The UME was immersed into the electrolyte solution and it was found (as it is normally) that a steady-state current of 1.2 nA was reached in cyclic voltammetry when a potential of 0.350 V was applied in the electrolyte solution. The steady-state current is proportional to the Fc concentration according to

$$i = 4nDFca \quad (1)$$

where D ($7.6 \times 10^{-6} \text{ cm}^2 \text{ s}^{-1}$) is the diffusion coefficient of the species detected, a (cm) is the electrode radius, c (mol cm^{-3}) is the concentration Fc, F (C mol^{-1}) is the Faraday constant and n is the number of electrons transferred per molecule.⁴⁹

The UME biased at 0.350 V, approached the CIGS substrate at 1 $\mu\text{m s}^{-1}$ until the UME current was 1.6 nA. A probe approach curve (PAC) was obtained by measuring the current versus tip-to-substrate distance during this process. The current was normalized by the tip current (eqn (1)) when the electrode was far away from the CIGS film substrate while the distance was normalized by the radius of the Pt UME. SECM images in the constant height mode were taken by recording the biased UME current versus its X , Y coordinates (256×256 pixels) at room temperature. Further PACs were recorded above various spots of interest on an SECM image by means of the closed-loop positioning system allowing the precise location of the UME.

Chemical reactivity at the substrate was quantified by determining the pseudo-first-order rate at which ferrocenium-methanol (Fc^+) was reduced back to Fc (Fig. 1a):

$$v = kc_{\text{Fc}^+} \quad (2)$$

where k is pseudo-first-order rate constant⁵⁰ and c_{Fc^+} is the concentration of Fc^+ .

Scanning photoelectrochemical microscopy (SPECM) was used to determine the photoreactivity of the CIGS substrate, where a quartz halogen illuminator lamp (M1-150, Fiber-Lite, Dolan-Jenner, Mississauga, ON), with a gooseneck light guide, was used to illuminate the CIGS substrate (Fig. 1b). The light power reaching the SECM cell was measured as 98.0 mW with a standard division of 1.9 mW. Images and PACs in SPECM experiments were acquired with a similar methodology to the SECM as described above.

The following chemicals were purchased and used without any further purification: indium(III) chloride (anhydrous, Aldrich, >98%), selenium tetrachloride (Aldrich, copper chloride (Aldrich, 97%), gallium chloride (anhydrous, Aldrich, 99.999%), urea (Aldrich, reagent grade, 98%), and choline chloride (Sigma, reagent grade, ≥98%). Reaction temperature was kept constant at 65.0 ± 0.1 °C by a circulating water bath (VWR, model 1130S, Mississauga, ON).

Simulation

The COMSOL multiphysics software (version 3.5a, COMSOL Inc., Boston, MA) was used to generate simulated PACs. The electrode, substrate surface geometries and boundary conditions in COMSOL were set based on our experimental conditions.^{34,52} For the irreversible reaction at the CIGS substrate (Fig. 1), the Fc flux is expressed as:

$$D \left[\frac{\partial c(r, z)}{\partial z} \right]_{z=-d} = k [c_0 - c(r, -d)] \quad (z = -d) \quad (3)$$

where the origin is at the center of the disk electrode, $-d$ represents the UME-to-substrate distance, r and z are the radial and height distance axes in two dimensional cylindrical coordinates, respectively. The bulk Fc concentration is c_0 and $c(r, -d)$ is the Fc concentration function in the gap between the UME and substrate. The Fc⁺ concentration was equal to $c_0 - c(r, -d)$, assuming that Fc was oxidized to Fc⁺ completely at the UME. For a PAC with a fixed k , the tip currents corresponding to more than 20 tip-to-substrate distances, d , were calculated. The PAC was obtained by plotting the normalized tip current *versus* normalized tip-to-substrate distance. A group of PACs with various k values were superimposed on to the experimental PAC and a k value was determined from the simulated PAC that matched the experimental value. Other details and the related theory can be found elsewhere.^{34,52}

Results and discussion

A typical cyclic voltammogram of the Cu–In–Ga–Se system in Reline with glass/Mo as the working electrode and two Pt

wires as the reference and the counter electrodes at 65 °C is presented in Fig. S1 (ESI§). The electrochemistry of the four salts system is very complex. Peter and coworkers studied the electrochemistry of the elements of copper, indium, gallium and selenium in Reline for the first time and they also reported CV for the Cu–In–Se system.³⁰ There are two alloys formed in the Cu–In–Se system corresponding to Cu–Se and Cu–In. The corresponding cathodic peaks are assigned to the features seen in Fig. S1 (ESI§). Marked peaks in Fig. S1 (ESI§) are in good agreement with reduction potentials reported by Peter *et al.* for elements and alloys.³⁰ The average redox potential of Fc using the same electrochemical system with Pt standard electrode instead of glass/Mo as the working electrode in Reline is about 0.340 V.

Three examples are listed in Table 1 to show the dependence of CIGS film compositions on the conditions of the cyclic voltammetry method. Among these three examples, both samples #1 and #2 have their film compositions close to that of stoichiometric CIGS films suitable for the production of solar cells. Table 2 demonstrates CIGS thin film composition results obtained by EDX when using one deposition bath for 10 consecutive electrodepositions. We can clearly see that in the first deposition, the CIGS thin film has stoichiometric composition with Ga/(Ga + In) equal to 0.4 and Se/Cu of about 2.0. If we use the same solution for the second deposition the selenium to copper ratio drops quickly. From the third deposition onwards, none of the deposited CIGS thin films are of the desired stoichiometric ratio as Se/Cu drops below 1.0 and Ga/(Ga + In) decreases to 0.2. Although in consequent depositions the films do not maintain the optimal stoichiometric ratio, Ga/(Ga + In) is somewhat in the preferred ratio range (0.2 to 0.4).^{4,5} We are investigating replenishing the solution in order to obtain a stoichiometric film on subsequent depositions.

Table 2 Examples of CIGS thin film composition when using one solution bath for 10 times

Run #	Composition	Ga/(Ga + In)
1	Cu _{1.0} (In _{0.6} , Ga _{0.4})Se _{2.2}	0.4
2	Cu _{1.0} (In _{0.7} , Ga _{0.3})Se _{0.9}	0.3
3	Cu _{1.0} (In _{0.7} , Ga _{0.3})Se _{0.6}	0.3
4	Cu _{1.0} (In _{0.8} , Ga _{0.2})Se _{0.6}	0.2
5	Cu _{1.0} (In _{0.8} , Ga _{0.2})Se _{0.6}	0.2
6	Cu _{1.0} (In _{0.9} , Ga _{0.1})Se _{0.6}	0.1
7	Cu _{1.0} (In _{0.9} , Ga _{0.1})Se _{0.6}	0.1
8	Cu _{1.0} (In _{0.8} , Ga _{0.2})Se _{0.5}	0.2
9	Cu _{1.0} (In _{0.8} , Ga _{0.2})Se _{0.5}	0.2
10	Cu _{1.0} (In _{0.8} , Ga _{0.2})Se _{0.6}	0.2

[] = mM in the bath composition Cu = 7.5, In = 45, Ga = 45, Se = 65.

Table 1 Examples of controlling film compositions of the one-pot electrodeposited CIGS films

Sample #	Bath composition				Film composition	Ga/(Ga + In) of the film
	[Cu]	[In]	[Ga]	[Se]		
1	7.5	55	50	60	Cu _{1.0} (In _{0.7} , Ga _{0.3})Se _{1.8}	0.3
2	7.5	55	45	60	Cu _{1.0} (In _{0.7} , Ga _{0.3})Se _{1.9}	0.3
3	7.5	45	45	65	Cu _{1.0} (In _{0.6} , Ga _{0.4})Se _{2.2}	0.4

[] = mM in the bath composition.

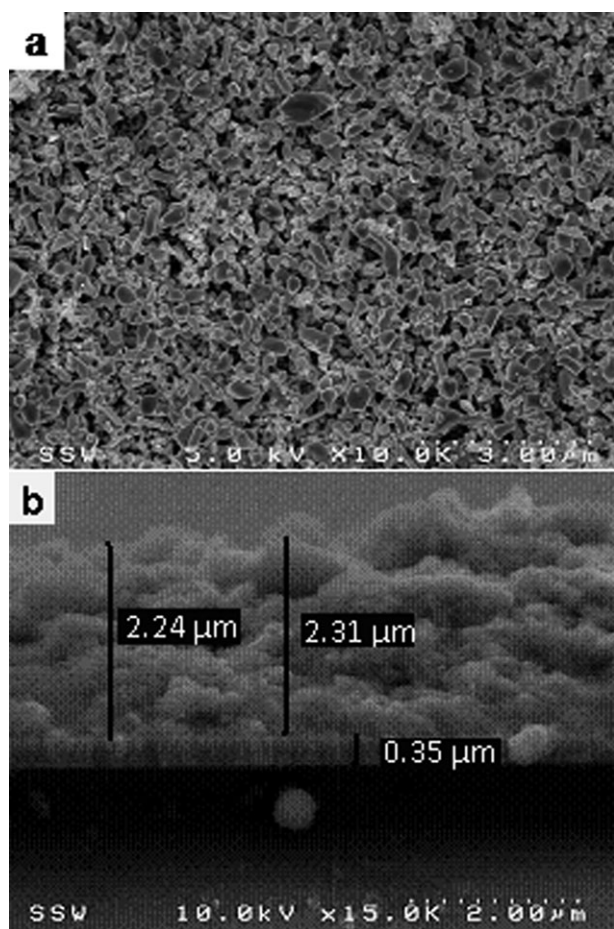


Fig. 3 (a) A typical SEM image and (b) a cross-section SEM image of the as-deposited thin film at a potential between -0.200 V and -2.200 V for 150 min, in 45 mM GaCl_3 + 65 mM SeCl_4 + 7.5 mM CuCl_2 + 45 mM InCl_3 solution at 65°C .

Fig. 3 illustrates the morphology of the as-deposited thin film during 150 min electrodeposition by means of CV. It shows that the thin film was compact and dense and the overall surface is covered by a relatively smooth layer of CIGS. Note that we did not observe formation of bubbles on the electrode or on the growing film during deposition and the films grown from these conditions were always crack-free. Good film stoichiometry was obtained according to the EDX results under the solution composition of 45 mM GaCl_3 + 60 mM SeCl_4 + 7.5 mM CuCl_2 + 55 mM InCl_3 which results in a thin film composition of $\text{Cu}_{1.0}(\text{In}_{0.7}, \text{Ga}_{0.3})\text{Se}_{1.9}$ (normalized by taking Cu equal to 1.0). Oxygen with an atomic percentage between 3 and 16 was detected in various films. It has been reported previously by Birkmire *et al.* that 15–17 atom% of oxygen was normally detected in most films.¹⁶ Fig. 3b shows a cross-section SEM image of the film. CV deposition allows the absorbing layer to have a thickness as high as $2.0\ \mu\text{m}$ which is favourable for efficient solar radiation absorption.

Formation of cauliflower-like florets was observed when the electrodeposition was carried out under constant potential at concentrations of Cu and Se higher than 10 mM and 75 mM, respectively. Fig. S2 (ESI \S) shows that the surface is covered

by cauliflower-like grains and large-sized clusters. Birkmire *et al.* showed that these phases are richer in Cu and Se.¹⁶ Our EDX results carried out on these areas showed that their composition is $\text{Cu}_{1.0}\text{Se}_{2.0}$ (Fig. S2d, ESI \S). Furthermore, EDX measurements carried out on spherical balls shown in Fig. S2a (ESI \S) indicate that they are pure selenium (Fig. S2c, ESI \S). These secondary phases are not favourable for fabricating photovoltaic devices as they may result in defects like shunt. These phases also survived high temperature postdeposition selenization treatment, but partially dissolved with aqueous KCN etching.¹⁶ The cyclic voltammetry deposition has a lower deposition rate as it deposits the elements in the forward course where the applied potential is scanned from 0 to negative direction, and then grains are refined in the reverse route where the potential is scanned back. In other words, using CV the cations are reduced and the semiconductor alloy is deposited onto the substrate in the forward scan, and some of the deposited CIGS is re-oxidized back to ions in solution in the reverse scan. In this way, the CV technique can generate higher quality CIGS grains than the constant potential method. Fig. 3 and Fig. S1 (ESI \S) demonstrate this trend. CV was done at 65°C and scan rate was $20\ \text{mV s}^{-1}$. Other technical considerations such as species diffusion, deposition rate control using constant-current method based on our knowledge on electrochemistry and surface chemistry will be discussed in a latter publication.

The TEM image of the CIGS thin film sample that was electrodeposited for 150 min using cyclic voltammetry at the bath temperature of 65°C is presented in Fig. 4. As can be seen from TEM image the CIGS thin film is indeed crystalline. Note that we did not post-treat these films with the exception of washing with water and drying with argon flow to remove solvent. They are as-deposited CIGS films.

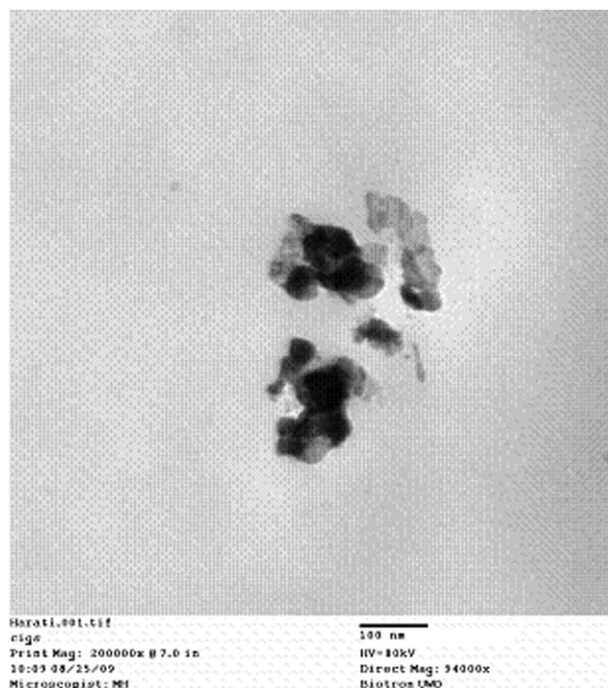


Fig. 4 TEM image of CIGS thin film.

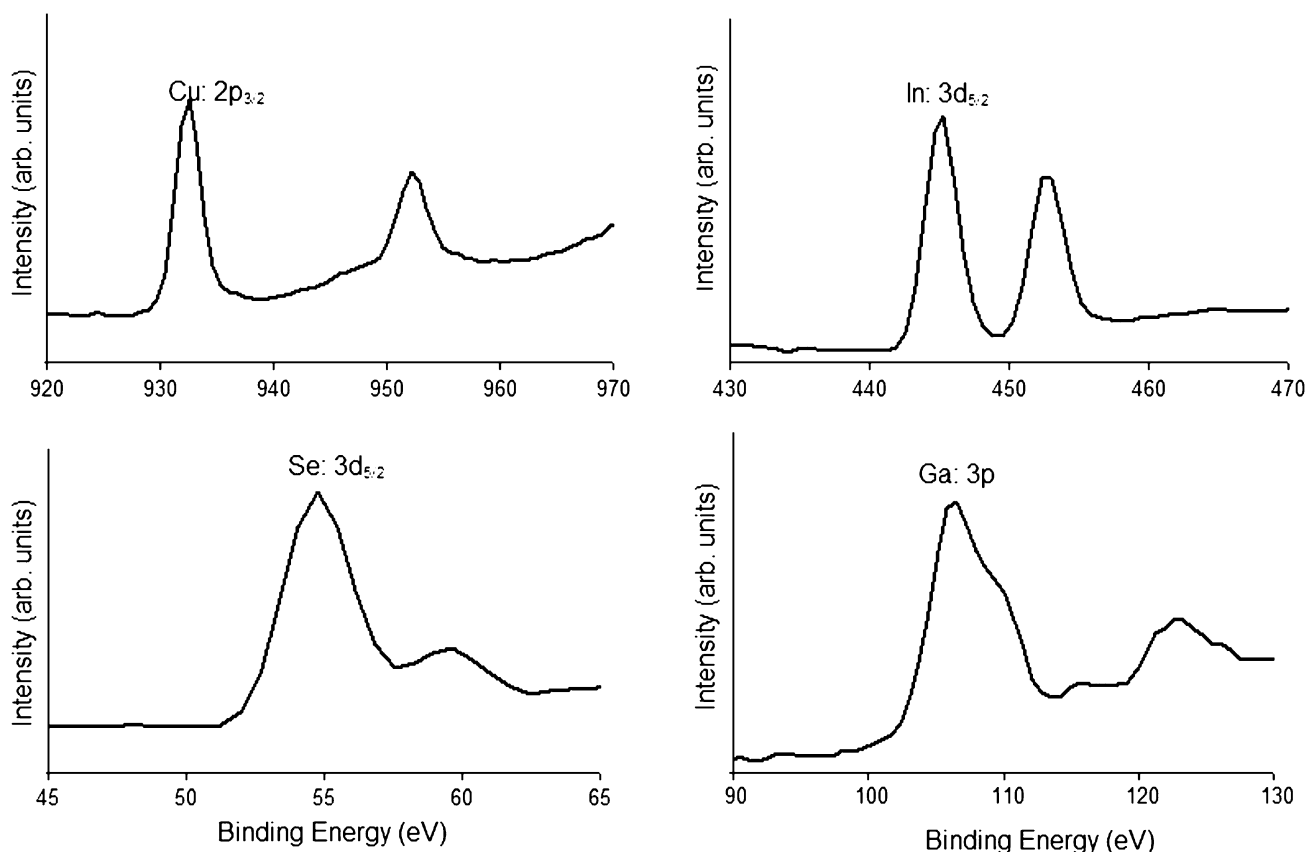


Fig. 5 Survey X-ray photoelectron spectra of Cu 2p, In 3d, Se 3d, Ga 3p regions for as-deposited CIGS film.

Fig. 5 presents X-ray photoelectron spectra of Cu 2p, In 3d, Se 3d, Ga 3p regions for as-deposited CIGS thin film. Binding energies are 932.55, 445.35, 105.85, and 54.75 eV for Cu 2p, In 3d, Se 3d, and Ga 3p, respectively, which is consistent with values reported by others.⁵⁵ Since the sample was exposed to air prior to the measurements, relatively high amounts of C- and O- on the surface were detected by XPS.¹⁶ We obtain quantitative information from the XPS survey to calculate film composition using the CasaXPS software. Analyzing the XPS survey shows that the composition of the thin film is $\text{Cu}_{1.0}(\text{In}_{0.7}, \text{Ga}_{0.3})\text{Se}_{2.1}$. The EDX and XPS analysis results indicate that all the four elements, *i.e.*, gallium, indium, selenium and copper are distributed uniformly over the surface and through the bulk of the film.

One of the most important qualities that a CIGS layer must have is high absorbance of sunlight. The absorbance of the films was examined by using UV-visible spectroscopy in the reflection mode and a Mo substrate was used as the reference. Fig. 6 shows the UV-visible absorption spectra in the wavelength range 400–900 nm for the as-prepared CIGS thin films using the cyclic voltammetry method at 65 °C for 150 minutes of deposition time. It can be seen that the absorbance is quite high in the measured wavelength range and that the maximum value is approximately 65% between 470 and 700 nm.

Fig. 7 depicts a Raman spectrum of a CIGS film measured at room temperature. The CIGS sample produces a Raman spectrum with a single intense scattering peak at 184 cm^{-1}

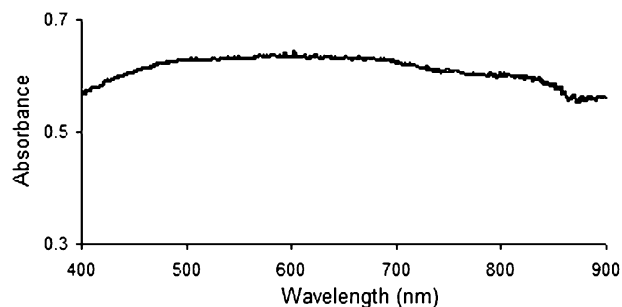


Fig. 6 UV-visible absorption spectra of the electrodeposited CIGS thin film on Mo/glass substrate at 65 °C for 150 min in Reline.

corresponding to the A_1 optical mode that is the characteristic peak of the chalcopyrite crystal structure.⁵⁶ In fact, A_1 mode represents the vibration of the Se in the x - y plane with the cations at rest. The position of this peak linearly increases with increasing Ga composition in the film. This spectrum also reveals mixed B2/E modes at approximately 246 cm^{-1} . An additional mode appears at 263 cm^{-1} , which is assigned to the A_1 mode of copper selenide (CuSe or Cu_2Se) phases in the sample. The inset in Fig. 7 illustrates the Confocal Raman image of the sample with the dimension of $50 \mu\text{m} \times 50 \mu\text{m}$. A complete Raman spectrum was recorded at each pixel. The Raman image was constructed by integrating the intensities of the above characteristic Raman bands in the scanned area. The Raman image demonstrates that the CIGS have the same

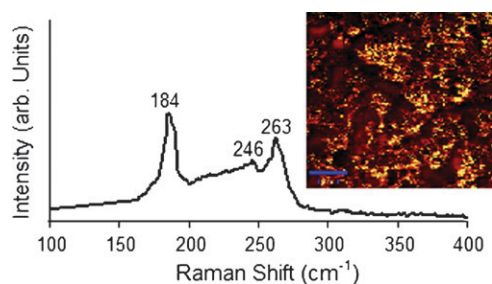


Fig. 7 A typical Raman spectrum of the CIGS thin film in Fig. 6 at room temperature with a Raman image in a $50 \mu\text{m} \times 50 \mu\text{m}$ area.

chemical structures. The dark spots signify a lower topography than bright ones. Note that the mapping represents a region of the absorber near the surface with a penetration depth of 100 nm.

Fig. 8 shows the SECM image of a CIGS substrate with thickness of $2 \mu\text{m}$ in a dark atmosphere and the SPECM image of the CIGS film under illumination. The two images were obtained by scanning the CIGS film substrate in a single area in constant height mode. The currents obtained under illumination (ranging from 1.72 to 1.95 nA) were higher than the currents obtained in the dark (ranging from 1.63 to

1.76 nA). This means that the reaction rate for Fc^+ reducing to Fc under illumination was higher than that in dark. Since SECM image and SPECM image were taken on a small scale, they seem to be not uniform. But the difference in current is very small. Actually on a large scale, the images of the film reactivity in dark and upon illumination are uniform.

Since the surface images included both topography and reactivity information of the CIGS film, PACs were then recorded at different spots on the surface in order to extract the reactivity from the topography. A PAC was obtained by measuring the current *versus* tip-to-substrate distance during this process. The current was normalized by the tip current when the electrode was far away from the CIGS film substrate while the distance was normalized by the radius of the Pt UME. Fig. 9 demonstrates typical experimental PACs in dark (a) and upon illumination (b) overlapped onto the set of simulated PACs with various rate constant values. The simulated PACs were generated following the procedure discussed briefly in the Simulation section. A certain k value was used in generating a PAC. Then the normalized current at each normalized distance was calculated in COMSOL³⁴, and a PAC of this specific k value was obtained in this way. Other PACs were simulated using various k values. It was found that the rate constant was 0.04 cm s^{-1} in the dark and 0.50 cm s^{-1}

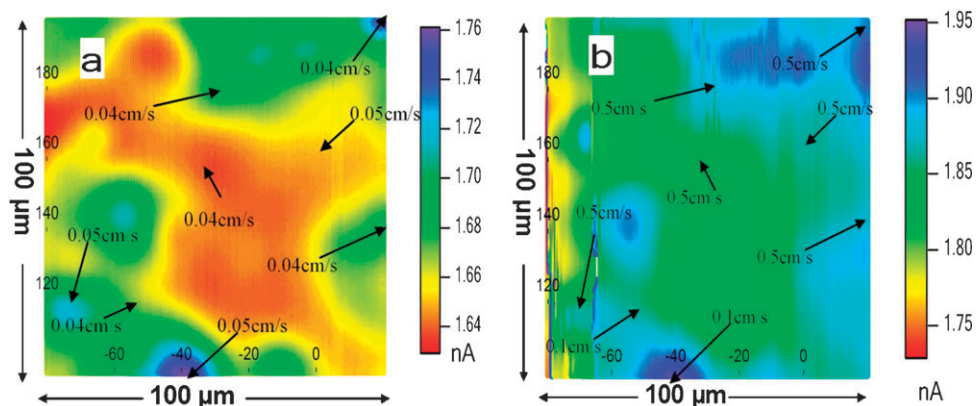


Fig. 8 SECM images ($100 \mu\text{m} \times 100 \mu\text{m}$) of surfaces of CIGS film substrate in dark (a) and under light (b). Imaging was carried out in a solution containing 0.9 mM ferrocenemethanol and 0.1 M Na_2SO_4 . The scanning electrode was a $10 \mu\text{m}$ Pt UME with an RG value of 3.0. Potential of 0.350 V was applied to the UME tip both in dark and under light. The arrows indicate k values of various spots on images in dark (a) and under light (b).

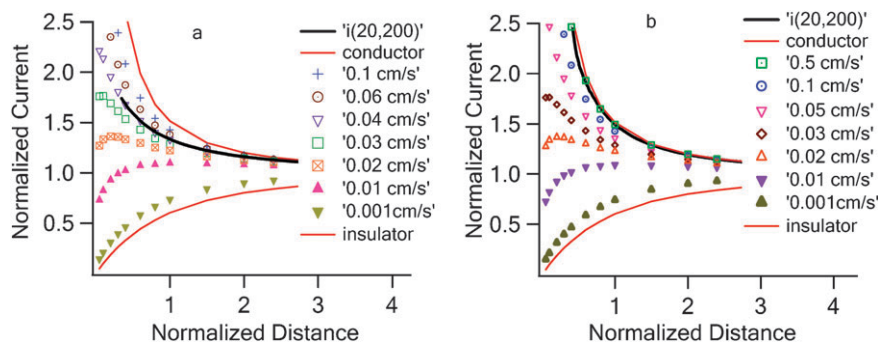


Fig. 9 An example of normalized probe approach curves (PACs) obtained above certain spot (20, 200) on the CIGS surface image superimposed on simulated PACs. (a) The experimental PAC in dark indicates that k value on this spot is 0.04 cm s^{-1} . (b) The experimental PAC under light indicates that k value on this spot is 0.5 cm s^{-1} .

upon illumination. These results agree well with SECM and SPECM images in Fig. 8. The pseudo-first-order rate constants determined in this way on various spots on the CIGS film are summarized on the two SECM images in Fig. 8. It was found that the rate constants in the dark varied from 0.04 to 0.05 cm s⁻¹ (Fig. 8a). This reflects that the reactivity at different spots on the surface is fairly similar, *i.e.* the surface reactivity is quite homogeneous. This observation agrees well with the Raman image in the inset of Fig. 7. Fig. 8b demonstrates that under illumination the pseudo-first-order rate constant of these spots on the CIGS varies from 0.10 to ~0.50 cm s⁻¹. The variation in the pseudo-first-order rate constants upon light irradiation is almost 10 times higher than those observed in the dark.

The rise of the current under illumination represents the high reactivity of the surface during UV/vis irradiation. When the CIGS film was in contact with a solution, the semiconductor/solution interface was formed.⁴⁹ A CIGS film is a p-type semiconductor. Before contact, the Fermi level in the CIGS p-type semiconductor is located near the energy E_v of the valence band edge. As shown in Fig. 2a, E_v lies below the Fermi level of the redox couple Fc^+ and Fc. When the CIGS film is in contact with the solution, electron transfer will occur at the interface until the Fermi levels in both phases are equal, as shown in Fig. 2b. In this case, equilibration occurs through electron transfer from the solution to the CIGS p-type semiconductor with the semiconductor becoming negatively charged.⁴⁹ The negative charge of CIGS film is distributed in a space-charge region, which causes the band energies to be more positive with increasing distance into the semiconductor. As a result, band bending occurs as shown in Fig. 2b. When the surface was irradiated with light with energy matched the band gap, E_g , photons were absorbed and electron-hole pairs were created. The electrons, moved to the surface at an effective potential according to the valence band edge, caused an efficient reduction of Fc^+ to Fc on the surface, as shown in Fig. 2c.⁴⁹ Thus the light irradiation to the CIGS p-type semiconductor surface promoted reduction of Fc^+ in the vicinity of the CIGS film and generated more Fc than in the dark case. As a result, the concentration Fc increased above the surface of CIGS film. According to eqn (1), this would cause a rise in current, which was recorded by UME in the proximity of the CIGS film surface. An increase in the rate constant was therefore observed.

Conclusions

In this work cations of Cu, In, Ga and Se were electrochemically reduced and deposited on a molybdenum electrode in one-pot format and a stoichiometric CIGS semiconductor alloy was formed at the electrode without the requirement of post-deposition thermal sintering. The cyclic voltammetry approach was found to generate better CIGS grains than the constant potential method. Reline was a cost-effective medium to avoid technical problems such as hydrogen generation in the aqueous solution, and its operating temperature is conveniently moderate which is suitable for application with polymers and other heat-sensitive substrates. Various microscopic and spectroscopic techniques were successfully

used to monitor the fabrication of the stoichiometric CIGS thin films. The reactivity and photoreactivity of the optimized CIGS film were quantified by the pseudo-first-order rate constants determined by SECM (in the dark) and SPECM (upon illumination).

Acknowledgements

We thank Brad Kobe (SEM/EDX) and Mark Biesinger (XPS) for use of instrument facilities at the Surface Science Western and Richard Glew at the Nanofabrication Laboratory at the University of Western Ontario. We acknowledge the financial support from Rosstech Inc., Ontario Centres of Excellence, the Natural Sciences and Engineering Research Council (CRD, i2i, New Discovery and Equipment Grants), Canada Foundation for Innovation, Ontario Innovation Trust, the Premier's Research Excellence Award, and the WORLDdiscoveries™ at Western. We are also grateful to Professor Richard J. Puddephatt for the gift of the conductivity apparatus. Technical assistance from John Vanstone, Jon Aukima, Patrick Therrien, Sherrie McPhee, Mary Lou Hart, Yves Rambahour and Barakat Misk is gratefully acknowledged.

References

- S.-H. Wei, S. B. Zhang and A. Zunger, *Appl. Phys. Lett.*, 1998, **72**, 3199–3201.
- Y. Q. Lai, F. Y. Liu, Z. A. Zhang, J. Liu, Y. Li, S. S. Kuang, J. Li and Y. X. Liu, *Electrochim. Acta*, 2009, **54**, 3004–3010.
- R. N. Bhattacharya, W. Batchelor, J. E. Granata, F. Hasoon, H. Wiesner, K. Ramanathan, J. Keane and R. N. Noufi, *Sol. Energy Mater. Sol. Cells*, 1998, **55**, 83–94.
- I. Repins, M. A. Contreras, B. Egaas, C. DeHart, J. Scharf, C. L. Perkins, B. To and R. Noufi, *Progr. Photovolt.: Res. Appl.*, 2008, **16**, 235–239.
- M. A. Contreras, B. Egaas, K. Ramanathan, J. Hiltner, A. Swartzlander, F. Hasoon and R. Noufi, *Progr. Photovolt.: Res. Appl.*, 1999, **7**, 311–316.
- P. S. Vasekar, A. H. Jahagirdar and N. G. Dhere, *Thin Solid Films*, 2010, **518**, 1788–1790.
- B. Canava, J. F. Guillemoles, J. Vigneron, D. Lincot and A. Etcheberry, *Proc. - Electrochem. Soc.*, 2006, **2003–32**, 31–40.
- W. Li, Y. Sun, W. Liu, F. Y. Li and L. Zhou, *Chin. Phys.*, 2006, **15**, 878–881.
- D. Rudmann, D. Brémaud, A. F. Da Cunha, G. Bilger, A. Strohm, M. Kaelin, H. Zogg and A. N. Tiwari, *Thin Solid Films*, 2005, **480–481**, 55–60.
- S. Schleussner, T. Kubart, T. Törndahl and M. Edoff, *Thin Solid Films*, 2009, **517**, 5548–5552.
- J. A. Hollingsworth, K. K. Banger, M. H. C. Jin, J. D. Harris, J. E. Cowen, E. W. Bohannon, J. A. Switzer, W. E. Buhro and A. F. Hepp, *Thin Solid Films*, 2003, **431–432**, 63–67.
- V. K. Kapur, A. Bansal, P. Le and O. I. Asensio, *Thin Solid Films*, 2003, **431–432**, 53–57.
- D. B. Mitzi, M. Yuan, W. Liu, A. J. Kellock, S. J. Chey, V. Deline and A. G. Schrott, *Adv. Mater.*, 2008, **20**, 3657–3662.
- M. G. Panthani, V. Akhavan, B. Goodfellow, J. P. Schmidtke, L. Dunn, A. Dodabalapur, P. F. Barbara and B. A. Korgel, *J. Am. Chem. Soc.*, 2008, **130**, 16770–16777.
- M. E. Calixto, P. J. Sebastian, R. N. Bhattacharya and R. Noufi, *Sol. Energy Mater. Sol. Cells*, 1999, **59**, 75–84.
- M. E. Calixto, K. D. Dobson, B. E. McCandless and R. W. Birkmire, *J. Electrochem. Soc.*, 2006, **153**, G521–G528.
- Y.-P. Fu, R.-W. You and K.-K. Lew, *J. Electrochem. Soc.*, 2009, **156**, E133–E138.
- J. P. Ao, L. Yang, L. Yan, G. Z. Sun, Q. He, Z. Q. Zhou and Y. Sun, *Acta Phys. Sin.*, 2009, **58**, 1870–1878.

- 19 F. Long, W. Wang, J. Du and Z. Zou, *J. Phys. Conf. Ser.*, 2009, **152**, 012074.
- 20 L. Zhang, F. D. Jiang and J. Y. Feng, *Sol. Energy Mater. Sol. Cells*, 2003, **80**, 483–490.
- 21 D. Xia, M. Xu, J. Li and X. Zhao, *J. Mater. Sci.*, 2006, **41**, 1875–1878.
- 22 D. Xia, J. Li, M. Xu and X. Zhao, *J. Non-Cryst. Solids*, 2008, **354**, 1447–1450.
- 23 J. Kois, M. Ganchev, M. Kaelin, S. Bereznev, E. Tzvetkova, O. Volobujeva, N. Stratieva and A. N. Tiwari, *Thin Solid Films*, 2008, **516**, 5948–5952.
- 24 S. Aksu, J. X. Wang and B. M. Basol, *Electrochem. Solid-State Lett.*, 2009, **12**, D33–D35.
- 25 B. M. Quinn, Z. Ding, R. Moulton and A. J. Bard, *Langmuir*, 2002, **18**, 1734–1742.
- 26 A. P. Abbott, G. Capper, D. L. Davies, R. K. Rasheed and V. Tambyrajah, *Chem. Commun.*, 2003, 70–71.
- 27 L. E. Barrosse-Antle, L. Aldous, C. Hardacre, A. M. Bond and R. G. Compton, *J. Phys. Chem. C*, 2009, **113**, 7750–7754.
- 28 D. E. Khoshtariya, T. D. Dolidze and R. Ven Eldik, *Chem.–Eur. J.*, 2009, **15**, 5254–5262.
- 29 D. Ragupathy, A. I. Gopalan and K. P. Lee, *Electrochem. Commun.*, 2009, **11**, 397–401.
- 30 D. D. Shivagan, P. J. Dale, A. P. Samantilleke and L. M. Peter, *Thin Solid Films*, 2007, **515**, 5899–5903.
- 31 A. J. Bard, in *Scanning Electrochemical Microscopy*, ed. A. J. Bard and M. V. Mirkin, Marcel Dekker, New York, 2001, pp. 1–17.
- 32 S. Amemiya, A. J. Bard, F.-R. F. Fan, M. V. Mirkin and P. R. Unwin, *Annu. Rev. Anal. Chem.*, 2008, **1**, 95–131.
- 33 Z. F. Ding, B. M. Quinn and A. J. Bard, *J. Phys. Chem. B*, 2001, **105**, 6367–6374.
- 34 R. Zhu, Z. Qin, J. J. Noel, D. W. Shoesmith and Z. Ding, *Anal. Chem.*, 2008, **80**, 1437–1447.
- 35 R. K. Zhu, S. A. Macfie and Z. F. Ding, *Langmuir*, 2008, **24**, 14261–14268.
- 36 F. Li, B. Su, F. C. Salazar, R. P. Nia and H. H. Girault, *Electrochem. Commun.*, 2009, **11**, 473–476.
- 37 S. Schwamborn, L. Stoica, X. X. Chen, W. Xia, S. Kundu, M. Muhler and W. Schuhmann, *ChemPhysChem*, 2010, **11**, 74–78.
- 38 D. Battistel, S. Daniele, R. Gerbasi and M. A. Baldo, *Thin Solid Films*, 2010, **518**, 3625–3631.
- 39 B. Liu, S. A. Rotenberg and M. V. Mirkin, *Proc. Natl. Acad. Sci. U. S. A.*, 2000, **97**, 9855–9860.
- 40 J. Mauzeroll, A. J. Bard, O. Owghadian and T. J. Monks, *Proc. Natl. Acad. Sci. U. S. A.*, 2004, **101**, 17582–17587.
- 41 P. M. Diakowski and Z. Ding, *Phys. Chem. Chem. Phys.*, 2007, **9**, 5966–5974.
- 42 C. Nowierski, J. J. Noel, D. W. Shoesmith and Z. F. Ding, *Electrochem. Commun.*, 2009, **11**, 1234–1236.
- 43 X. Zhao, S. Lam, J. Jass and Z. Ding, *Electrochem. Commun.*, 2010, **12**, 773–776.
- 44 E. M. El-Giar, R. A. Said, G. E. Bridges and D. J. Thomson, *J. Electrochem. Soc.*, 2000, **147**, 586–591.
- 45 G. Wittstock, *Fresenius J. Anal. Chem.*, 2001, **370**, 303–315.
- 46 B. B. Katemann, A. Schulte and W. Schuhmann, *Chem.–Eur. J.*, 2003, **9**, 2025–2033.
- 47 R. K. Zhu, S. B. Xu, G. Podoprygorina, V. Boehmer, S. Mittler and Z. F. Ding, *J. Phys. Chem. C*, 2008, **112**, 15562–15569.
- 48 A. J. Bard, *J. Photochem.*, 1979, **10**, 59–75.
- 49 A. J. Bard and L. R. Faulkner, *Electrochemical Methods: Fundamentals and Applications*, John Wiley & Sons Inc., New York, 2nd edn, 2001.
- 50 S. K. Haram and A. J. Bard, *J. Phys. Chem. B*, 2001, **105**, 8192–8195.
- 51 F. P. Wang, X. T. Zhou, J. G. Zhou, T. K. Sham and Z. F. Ding, *J. Phys. Chem. C*, 2007, **111**, 18839–18843.
- 52 C. Nowierski, J. J. Noel, D. W. Shoesmith and Z. Ding, *Electrochem. Commun.*, 2009, **11**, 1234–1236.
- 53 R. Zhu and Z. Ding, *Can. J. Chem.*, 2005, **83**, 1779–1791.
- 54 R. Zhu, S. M. Macfie and Z. Ding, *J. Exp. Bot.*, 2005, **56**, 2831–2838.
- 55 J. Yang, Z. Jin, C. Li, W. Wang and Y. Chai, *Electrochem. Commun.*, 2009, **11**, 711–714.
- 56 W. Witte, R. Kniese and M. Powalla, *Thin Solid Films*, 2008, **517**, 867–869.